

Study of antiferromagnetic resonance in EuTe by the method of inelastic scattering of light

A. S. Borovik-Romanov, S. O. Demokritov, N. M. Kreines, and V. I. Kudinov

Institute of Physics Problems, USSR Academy of Sciences

(Submitted 1 October 1984)

Zh. Eksp. Teor. Fiz. **88**, 1348–1358 (April 1985)

The method of inelastic scattering of light is used to investigate AFMR in the cubic two-sublattice antiferromagnet EuTe in a wide range of magnetic fields (up to 65 kOe). Resonance with the soft mode was observed near the spin-flip transition. The AFMR spectrum is calculated for arbitrary directions and values of the magnetic field. The dynamic-susceptibility tensor and the oscillation modes at resonance are determined.

§1. INTRODUCTION

Since its discovery¹ in 1951, antiferromagnetic resonance (AFMR) has become a powerful means of studying the dynamics of antiferromagnets (AF). Since most AF have a magnetic-ordering temperature $T_N \gtrsim 10$ K and accordingly an exchange field $H_E \gtrsim 10^5$ Oe, AFMR experiments are usually performed under conditions when $H \ll 2H_E$. It is of definite interest to study the resonance spectrum in magnetic fields up to $H_{sf} = 2H_E$ at which the AF goes over into the paramagnetic phase (spin-flip transition).

The first experimental data on this subject have been reported quite recently.² The AFMR spectrum was measured in fields up to $2H_E$ in a $(C_2H_5NH_3)_2CuCl_4$ crystal. This substance is a quasi-two-dimensional system; the ferromagnetic exchange in a plane is larger by several orders than the antiferromagnetic exchange between planes. Therefore the spin-flip field H_{sf} , which is determined by the weak antiferromagnetic exchange, is anomalously small, 1.6 kOe. The AF-transition temperature $T_N = 10.2$ K is determined by the stronger ferromagnetic exchange. The relatively weak spin-flip field and the rather high magnetic-ordering temperature have enabled the authors of Ref. 2 to measure the AFMR spectrum in the entire range of fields in which antiferromagnetic order exist.

We investigate in this paper the AFMR spectrum in magnetic fields up to H_{sf} in the easy-plane antiferromagnet EuTe. This europium chalcogenide is a magnetic semiconductor.^{3,4} In contrast to the quasi-two-dimensional AF investigated in Ref. 2, EuTe is a Heisenberg AF isomorphic to the classical MnO.

We investigated the AFMR spectrum by the method of Brillouin scattering (BS) of light in a direct-scattering geometry. Such investigations are referred to also as light modulation by magnetic resonance (see, e.g., Ref. 5).

The macroscopic dynamics of the easy-plane AF was calculated on the basis of the Landau-Lifshitz equations for the case when the external field has arbitrary magnitude and direction relative to the easy plane. Expressions were obtained for the AFMR spectrum and for the generalized dynamic-susceptibility tensor, and the oscillation modes of the ferro- and antiferromagnetic vectors were determined. The easy-plane anisotropy field H_A was determined by a best fit of the calculated and measured spectra.

§2. SAMPLES AND TECHNIQUE

Europium chalcogenide have a cubic crystal structure of the NaCl type, and their symmetry is described by the space group O_h^5 . When the temperature is lowered they go over into various magnetically ordered states. The magnetic properties of the pure compounds are governed by the strongly localized moment of the rare-earth ion Eu^{2+} (electron configuration $4f^7$) whose spin $s = 7/2$ and whose orbital angular momentum $L = 0$. EuTe is an antiferromagnet. Its magnetic order was investigated by many. Heat-capacity measurements yield a transition temperature $T_N = (9.64 \pm 0.06)$ K (Ref. 6). Neutron-diffraction experiments⁷ have shown that the AF order in EuTe is similar to the cubic face-centered AF structure of MnO, viz., the spins lie in an (111) plane (the easy plane), and the spins in two planes are oppositely directed. Since a cubic crystal has four equivalent (111) planes, the crystal breaks up below T_N in two AF domains, viz., twin (T) domains. The crystal cannot be transformed into a one-domain one by an external magnetic field. The easy-plane anisotropy that tends to locate the spins in the (111) plane is due to dipole-dipole interaction.^{8,9} The effective anisotropy field H_A is 8 kOe (Ref. 10). A weak intraplanar anisotropy is present in the (111) easy plane and aligns the spins in the [112] direction (the anisotropy field in the easy plane is $H = 8$ Oe). Each (111) plane contains three equivalent [112] directions, so that each T domain can contain six so-called S (for spin) domains.

Exchange interaction in a pure stoichiometric EuTe sample is described by the interaction of each Eu^{2+} ion with twelve nearest neighbors and with six ions from the next coordination sphere. The spin interaction is ferromagnetic with the nearest neighbors, and antiferromagnetic with next-nearest. The effective exchange field is $H_E = 36$ kOe. In a magnetic field $H_{sf} = 2H_E = 72$ kOe (at $T = 0$) EuTe goes from the AF into the paramagnetic phase (spin-flip transition). The saturation magnetization $4\pi M_0$ reaches then 11.6 kOe.¹¹

The AFMR spectrum of EuTe was investigated in relatively weak magnetic fields up to 24 kOe at frequencies 9.18 and 24 GHz.¹⁰ The microwave-power absorption was recorded as a function of the external magnetic field. Several resonances were observed, corresponding to different T domains. It was shown that the field dependence of the AFMR

frequency at $H \ll H_{sf}$ is given approximately by $\omega = \gamma H \sin \varphi$, where φ is the angle between the C_3 axis and the direction of the external magnetic field.

EuTe is a semiconductor. At sufficiently high density, the conduction electrons can influence substantially the magnetic ordering via the s - f exchange. For example, they can give rise to weak ferromagnetism.^{4,11,12} According to Ref. 11, a substantial change of the magnetic order sets in at a free-electron density $n_{ef} \cdot 10^{19}$ – 10^{20} cm⁻³. At the light wavelength $\lambda = 632.8$ nm used in our experiment the EuTe crystals are relatively transparent: the penetration depth is ~ 70 μ m. In the ordered state, EuTe exhibits strong magneto-static effects. Thus the Faraday effect (Φ) at saturation reaches $\sim 10^5$ deg/cm at $T = 2$ K, in agreement with the data of Ref. 13. We have used in the present study EuTe crystals which L. A. Klinkova has grown gas-transport reaction method at the Institute of Solid State Physics of the USSR Academy of Sciences.

The samples were plates whose two natural cleaved surfaces were with (100) planes. The experiments were performed on three samples. The main results were obtained with a sample measuring $0.3 \times 0.7 \times 0.7$ mm. The crystal position in the cryostat was adjusted by a laser beam reflected from the cleaved surface of the sample. The orientation error did not exceed $\sim 1^\circ$.

By comparing the measured resistances of our samples with the results of Ref. 11 we found the free-carrier densities in our case to be of the order of 10^{15} cm⁻³. According to Ref. 11, it can be assumed that the conduction electrons do not distort the initial antiferromagnetic structure of the investigated crystals. This assumption was confirmed by magnetic measurements on our samples, which failed to reveal, accurate to $10^{-3} M_0$, any weak ferromagnetic moment in a zero magnetic field.

The AFMR in EuTe was recorded by using Brillouin scattering of light in a direct-scattering geometry. The spectrum of light passing through a crystal in which magnetic resonance is excited is known⁵ to contain, besides the unshifted frequency Ω , two satellites with frequencies $\Omega \pm \omega$, where Ω and ω are respectively the frequencies of the incident and resonant light. The intensities of the satellites are determined, other conditions being equal, by the square of the alternating component of the magnetic moment. Thus, the location and other features of the resonance can be determined from the dependence of the inelastic-light scattering intensity on the magnetic field.

To study the AFMR in EuTe at low temperature by the

Brillouin-scattering method we used apparatus consisting of three principal parts (Fig. 1):

a) An optical system consisting of a high-contrast high-resolution spectrometer. The operation of this part will be discussed in detail below.

b) A pass-through microwave spectrometer for 35–45 GHz with tunable cylindrical resonator. The resonator Q was $(2-3) \cdot 10^3$. The sample was placed on the axis of the cylindrical cavity at the antinode of the microwave-field magnetic component. Special openings of 1 mm diam were cut in the resonator walls to permit passage of the light. The microwave power (P_{micr}) sources were either a ~ 1 W magnetron or ~ 5 mW klystrons. The spectrometer permitted resonance excitation in the crystal and measurement of the power it absorbed.

3) Optical helium cryostat with a horizontal superconducting solenoid. The cryostat permitted operation in superfluid ⁴He at a temperature < 2 K. The maximum magnetic field produced by the solenoid at a current ~ 100 A was 65 kOe. To operate with such current in the pumped-out cryostat (vapor pressure ~ 10 Torr), special current leads with large heat-exchange surface were made (by soldering disks on the leads). Their construction increased insignificantly the evaporability of the helium in the cryostat. The magnetic field was measured with a low-temperature Hall pickup. For a more accurate determination of the field in which the sample was located, the Hall-pickup readings were calibrated against the ESR signal in DPPH placed alongside the crystal.

We turn now to the operation of the optical part of the apparatus. Its construction is general outline is the same as of that described in detail in Refs. 5 and 14. A number of important later modification extended its capabilities.

The light source was an LG-38 laser generating ~ 40 mW at a wavelength $\lambda = 632.8$ nm. The spectral instrument was a Burleigh scanning five-pass Fabry-Perot interferometer (FPI) with a contrast $> 10^8$. The data were stored and recorded, and the FPI adjusted and scanned, using the Burleigh DAS-1 system. For continuous recording of the dependence of the light-signal intensity on an external parameter (microwave power, magnetic field temperature, temperature) we have added a recording system based on the Ortec Brookdale photon counting system (PC). The latter was connected to one of the two independent outputs of the discriminator-preamplifier (DP) that received the signal from the photomultiplier (PM) (see Fig. 1). The signal from the second DP output was fed to the DAS-1 system. The photon

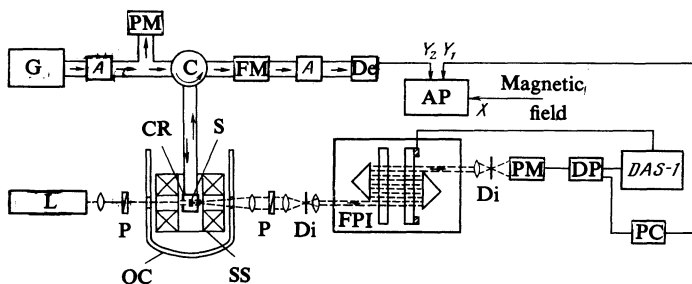


FIG. 1. Overall diagram of experimental setup: G—microwave oscillator, A—attenuator, PM—power meter, C—circulator, FM—frequency meter, De—detector, P—polarizer, Di—diaphragm, FPI—Fabry-Perot interferometer, DP—preamplifier, PC—photon counter, AP—automatic plotter, L—laser, CR—cavity resonator, S—sample, SS—superconducting solenoid, OC—optical cryostat.

counter counted the number of photons recorded by the PM in a definite time interval (usually 1 s) and displayed it as an analog voltage on an automatic plotter.

The measurement procedure was the following. As already indicated, the spectrum of the scattered light passing through the FPI contained two satellites of substantially lower intensity, shifted by the resonance frequency $\Delta\Omega = \pm\omega$ (Fig. 2). The displacement of the movable mirror of the FPI was decreased in amplitude to cause the interferometer to pass only one of these satellites. The relatively high satellite intensity could be used by the DAS-1 system to adjust the FPI and permitted thus prolonged experiments. In this regime, the FPI serves in fact as an extremely narrow-band tunable high-contrast filter for the displaced frequency. The photon counter recorded the number of photons fed to the PM during one scan of the FPI. This number is proportional to the satellite intensity. The information obtained was fed to a digital display and to the Y_1 coordinate of the plotter. The plotter Y_2 coordinate received simultaneously a signal proportional to the microwave power absorbed in the resonator. The plotter X coordinate was fed a Hall-pickup voltage proportional to the magnetic field intensity. As a result, the resonance line could be determined simultaneously from the microwave-power absorption and from the change of the inelastic light-scattering intensity. A typical experimental plot of the scattered-light intensity vs the magnetic field, up to 65 kOe, for AFMR in EuTe is shown in Fig. 3. The X coordinate of the plotter could also receive signals determined by other parameters, such as microwave power.

The procedure developed for continuous recording of the scattered-light intensity not only facilitated greatly the experiment, but also improved substantially the measurement accuracy.

Introduction of double registration of the light-signal intensity has thus considerably expanded our capabilities. It enabled us to record simultaneously light with shifted frequency, adjust the FPI, and record continuously the dependences of the scattered-light intensity on external parameters.

It should also be noted that the presence of strong magneto-optic effects in relatively transparent EuTe crystals has made this method of recording AFMR highly sensitive. At resonance, with exciting microwave power 1 W, the maximum useful signal/noise ratio was $\sim 2 \cdot 10^3$.

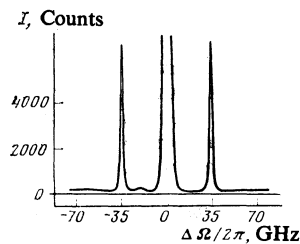


FIG. 2. Spectrum of light passing through an EuTe sample in which AFMR was excited. $\lambda_{\text{light}} = 632.8$ nm, $T = 1.8$ K, $\omega_{\text{micro}} = 35.2$ GHz, $P_{\text{micro}} \approx 5$ mW.

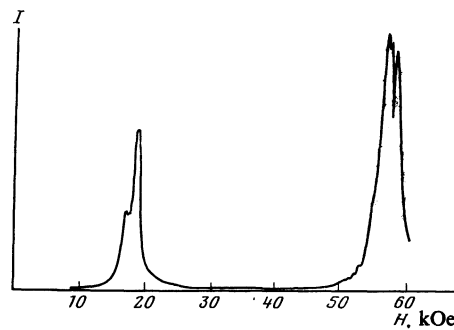


FIG. 3. Scattered-light intensity I vs the magnetic field H for AFMR in EuTe; $\omega_{\text{micro}} = 35.2$ GHz, $P_{\text{micro}} = 200$ mW, $T = 1.8$ K.

§3. EXPERIMENTAL RESULTS

The AFMR in EuTe was investigated by us at four frequencies, $\omega/2\pi = 35.2, 39.7, 42.6,$ and 44.7 GHz. We used two experimental geometries (see Fig. 1): 1) $\mathbf{h}_{\text{micro}} \perp \mathbf{H}/\mathbf{k}_{\text{inc}}$ and 2) $\mathbf{h}_{\text{micro}} \perp \mathbf{H} \perp \mathbf{k}_{\text{inc}}$. Resonance was observed both in weak fields and in fields close to $2H_E$ (Fig. 3). At arbitrary field direction relative to the crystal axes, several resonance lines were observed in both the low and high frequency regions; this corresponds to resonances in different T domains. The latter existed in all the available magnetic fields. When the field was oriented along the $[100]$ axis all the T domains turned out to be in equivalent positions and the resonance lines corresponding to them were superimposed. The structure of the resonance lines in Fig. 3 is due to inexact equality of the resonances in the different T domains, brought about by the insufficiently exact crystal orientation (error $\sim 1^\circ$).

The light-scattering intensity in AFMR depended little on the experimental geometry and was approximately equal for the two resonant fields.

Note that when the AFMR was recorded in EuTe the microwave spectrometer recorded distinctly only the weak-field resonance. Reliable recording of the strong-field resonance with our spectrometer was difficult, apparently because of the insufficient stability of the oscillator. The strong-field resonance was therefore recorded by the optical method. The microwave plots weak-field AFMR linewidth were identical.

The resonance field obtained in experiment for the cited frequencies are marked by points in Fig. 5. A study of the dependence of the scattered-light intensity on the applied microwave power in a fixed resonant field has shown that at 50 mW power the resonance begins to saturate and become nonlinear. The saturation of the resonance is apparently due

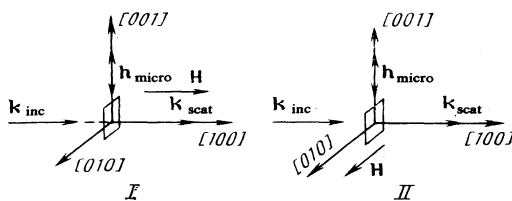


FIG. 4. Experimental geometries employed: I—geometry 1, II—geometry 2; $\mathbf{k}_{\text{inc}}, \mathbf{k}_{\text{scat}}$ —wave vectors of incident and scattered light.

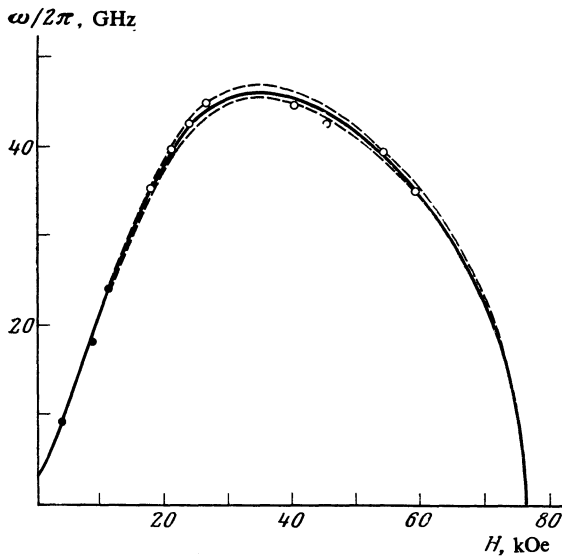


FIG. 5. Spectrum of low-frequency AFMR branch in EuTe at $\mathbf{H} \parallel [100]$ ($\varphi = 54.7^\circ$): \circ —present data, \bullet —data of Ref. 10. The solid line shows the AFMR spectrum calculated with allowance for the following demagnetizing factors: $N_x = N_y = 0.25$; $N_z = 0.5$. The dashed lines show the corridor error due to the inaccurate orientation of the crystal C_4 axis ($\pm 1^\circ$) relative to the magnetic field H .

to overheating of the spin system. We note also that inelastic light scattering was recorded not only in fields close to resonance, but also at any value of magnetic field, including $H = 0$. This scattering is due to the nonresonant susceptibility of the magnetic system. An investigation of the polarization of the inelastically scattered light has shown that, in the main, the scattering is not accompanied by rotation of the polarization plane.

§4. CALCULATION OF HIGH-FREQUENCY DYNAMICS OF EASY-PLANE ANTIFERROMAGNET

A. Model and calculation method

The AFMR spectrum of an easy-plane AF was calculated in detail in Ref. 15. For a comparison with our experimental results, however, account had to be taken of the demagnetizing factor. We have therefore analyzed the high-frequency dynamics of an easy-plane AF on the basis of the macroscopic Landau-Lifshitz equations.^{16,17} As a result, besides the AFMR spectrum, we obtained an expression for the dynamic susceptibility tensor and determined the oscillation modes.

Confining ourselves to low temperatures, we assume conservation of the sublattice magnetization:

$$|\mathbf{M}_1| = |\mathbf{M}_2| = M_0/2, \quad (1)$$

where M_0 is the saturation magnetization. We express the free-energy density of the easy-plane AF magnetic system in the form

$$F = -\frac{\delta}{2} \mathbf{L}^2 + \frac{K}{2} L_z^2 - \frac{K_1}{2} L_y^2 - \mathbf{H}^{(i)} \mathbf{M} - \mathbf{h}_m \mathbf{m} - \mathbf{h}_l \mathbf{l}, \quad (2)$$

where

$$\delta > 0, \quad K > 0, \quad K_1 > 0, \quad \mathbf{M} = \mathbf{M}_1 + \mathbf{M}_2, \quad \mathbf{L} = \mathbf{M}_1 - \mathbf{M}_2.$$

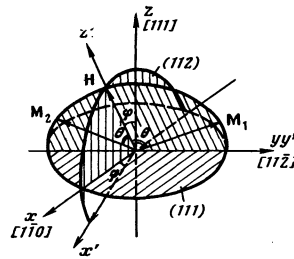


FIG. 6. Coordinate frames used in the calculation: (x, y, z) is connected with the crystallographic axis $[111]$, $z \parallel [111]$; $x \parallel [110]$, while (x', y', z') is connected with the magnetic-field direction.

The free energy is expressed in a coordinate frame (x, y, z) attached to the (111) plane in accordance with Fig. 6. The following phenomenological constants are used in (2): the antiferromagnetic-exchange constant δ connected with the effective exchange field $H_E = \delta M_0/2 = 36$ kOe (Ref. 11); the easy-plane anisotropy constant due to the dipole-dipole interaction^{8,9}; $H_A = K M_0 = 8$ kOe; the constant K_1 of the intraplanar anisotropy $H_a = K_1 M_0 = 8$ Oe; the constant internal magnetic field $\mathbf{H}^{(i)}$ [$H^{(i)} = H^{(e)} - 4\pi N_3 M$, where N_3 is the demagnetizing factor along \mathbf{M}]. We consider the case when the magnetic field is applied in the (112) plane, i.e., perpendicular to the anisotropy axis in the easy plane (see Fig. 6). Next, \mathbf{m} and \mathbf{l} are the time-dependent components of \mathbf{M} and \mathbf{L} , while \mathbf{h}_m and \mathbf{h}_l are generalized forces that correspond to the variables \mathbf{m} and \mathbf{l} (Ref. 18). In the absence of fluctuations, for example, \mathbf{h}_m coincides with the homogeneous part of the alternating high-frequency field acting on the sample, and \mathbf{h}_l can be regarded as a magnetic field whose sign differs at the locations of ions belonging to different sublattices.

Since the results obtained for strong magnetic fields are easier to deal with in a coordinate frame fixed in the field, we introduce new coordinate axes such that $z' \parallel \mathbf{H}$, and the arrangement of the other axes is shown in Fig. 6.

B. Equilibrium state of easy-plane AF. AFMR spectrum. Generalized tensor of dynamic susceptibility

From the condition that the free energy be a minimum, and taking (1) into account, we obtain the equilibrium values of \mathbf{M} and \mathbf{L} (at $H_a \ll H, H_E$):

$$\begin{aligned} \mathbf{M} &= M_0 \mathbf{H}^{(i)} / 2H_E, \quad L_x = L_z = 0, \\ L_y &= M_0 (1 - (H^{(i)} / 2H_E)^2)^{1/2} \quad (H^{(i)} < 2H_E). \end{aligned} \quad (3)$$

We see hence that the AF magnetization is directed along the magnetic field and is proportional to its modulus H up to the field $2H_E$ at which the magnetic sublattices collapse and the moment of the system saturates. The static susceptibility is isotropic in this system: $\chi = M_0 / 2H_E$.

We have used the Landau-Lifshitz equations to solve the problem of small oscillations of the magnetic- and ferromagnetic-moment vectors \mathbf{m} and \mathbf{l} , and to determine the resonance frequencies and the dynamic susceptibility generalized relative to the frequencies introduced in (2). From the condition that the system of equations have upon lineariza-

tion a nontrivial solution we can obtain the frequencies of the natural oscillations in the system [see (A2) in the Appendix]. The AFMR spectra for certain fixed AFMR frequencies φ calculated from (A2) using the known constants for EuTe are shown in Fig. 7. The equation (A2) for the AFMR frequencies agree with those obtained in Refs. 15 and 19 if we put $H_a = 0$, $N_1 = N_2 = N_3 = 0$ in (A2).

The spectrum was calculated earlier for the particular cases when (a) $\varphi = 0$ and \mathbf{H} is perpendicular to the easy axis and (b) $\varphi = \pi/2$ and \mathbf{H} is in the easy plane (see Turov's monograph²⁰). We obtained

$$\omega_1 = \gamma(2H_E H_a)^{1/2} [1 - (H/2H_E)^2], \quad \omega_2 = \gamma(2H_E H_a + H^2)^{1/2}; \quad (4A)$$

at $\varphi = 0$ and

$$\omega_1 = \gamma H, \quad \omega_2 = \gamma [2H_E H_a (1 - H/2H_E)^2]^{1/2} \quad (4B)$$

at $\varphi = \pi/2$ (γ is the gyromagnetic ratio). Our equations agree exactly with the already known ones.

The tensor of the generalized dynamic susceptibility of an easy-plane AF was calculated on the basis of the Landau-Lifshitz equations relative to the generalized forces \mathbf{h}_m and \mathbf{h}_l introduced in Eq. (2), in the coordinate from (x' , y' , z') attached to the field (see Fig. 6). This tensor is defined as follows:

$$\begin{aligned} x_i(\omega) &= \chi_{ij}(\omega) f_j(\omega), \\ x &= (m_x', m_y', m_z', l_x', l_y', l_z'), \\ f &= (h_{x'}^m, h_{y'}^m, h_{z'}^m, h_{x'}^l, h_{y'}^l, h_{z'}^l). \end{aligned} \quad (5)$$

Here \mathbf{x} are the variable deviations of the vectors \mathbf{M} and \mathbf{L} from the static values as projected on the axes x' , y' , and z' ; \mathbf{f} is a generalized force, whose first three projections comprise the alternating magnetic field. The form of the tensor $\chi_{ij}(\omega)$ is given in Appendix (A3). The left- and right-hand sides of the tensor χ_{ij} ($j \leq 3$) describe the respective responses of the system to the alternating magnetic field and to the generalized force \mathbf{h}_l acting on the antiferromagnetic moment. The susceptibility-tensor block χ_{ij} ($i \leq 3; j \leq 3$) is the high-frequency magnetic-susceptibility tensor. The generalized dynamic susceptibility [see (A3)] describes fully the entire linear macroscopic dynamics of the magnetic system.

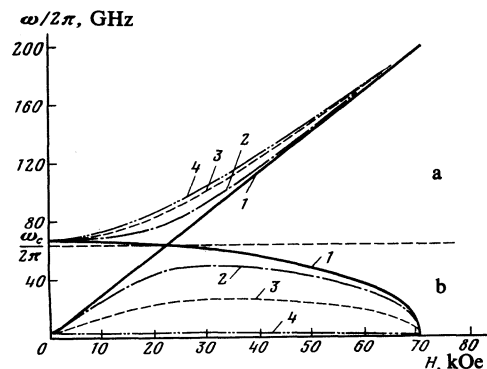


FIG. 7. Calculated spectrum (a—HF branch, b—LF branch) of AFMR in EuTe for four different direction of the field H in the $(11\bar{2})$ plane: 1 — $\varphi_1 = 90^\circ$; 2 — $\varphi_2 = 60^\circ$; 3 — $\varphi_3 = 30^\circ$; 4 — $\varphi_4 = 0$.

C. Oscillation modes in AFMR

From the calculated tensor of the generalized dynamic susceptibility (A3) and from Eq. (5) we have determined the AFMR oscillation modes as functions of the magnitude and direction of the magnetic field. The relative oscillation amplitudes of the vectors \mathbf{M} and \mathbf{L} are shown in Fig. 8 for certain directions of the field \mathbf{H} . The high- and low-frequency branches pertain to the frequencies $\omega > \omega_c$ and $\omega < \omega_c$, respectively.

Note that if condition (1) is satisfied we have only four independent variables among the six components of \mathbf{m} and \mathbf{l} , corresponding to four degrees of freedom in the system considered. Thus, l_y and l_z are not independent variables. They satisfy the relations

$$l_y = -m_z \operatorname{ctg} \theta, \quad l_z = -m_y \operatorname{tg} \theta, \quad (6)$$

where 2θ is the angle between M_1 and M_2 (see Fig. 6). It is known (see Fig. 8) that in an AF (in contrast to a ferromagnet) oscillations of the magnetic moment with change of its magnitude are possible in first-order approximation (longitudinal oscillations of M). The sublattice magnetic moments oscillate then relative to one another. If the magnetic field H lies in the easy plane ($\varphi = \pi/2$) we have $m_z = 0$ for ω_1 [see (4B)] and the magnetic cell oscillates as a unit. For ω_2 (4B) we have $m_z \neq 0$ and the sublattice magnetic moments oscillate relative to each other, and this leads to variation of \mathbf{M} .²¹ At an arbitrary magnetic-field direction, however, longitudinal m_z oscillations will be present in both AFMR branches. We point out that in Fig. 8 for the low-frequency branch the plane of the circle swept by the vector \mathbf{M} is not perpendicular to \mathbf{H} , meaning also \mathbf{M} , and this leads already to longitudinal oscillations of the vector \mathbf{M} in this case (see Fig. 8a).

§5. DISCUSSION OF EXPERIMENTAL RESULTS. COMPARISON OF EXPERIMENT WITH CALCULATION

We proceed to calculate the experimental results (§3) with the presented (§4) calculation of the high-frequency dynamics of an easy-plane AF.

Figure 5 shows the measured frequency dependence of the resonance field for the low-frequency (LF)¹ AFMR branch in the first experimental geometry (see Fig. 4). The calculated spectrum is shown by the solid curve. The phenomenological constants used in the calculation were $2H_E = 70.5$ kOe at $T = 1.8$ K (Ref. 11) and $H_a = 8$ Oe. The effective anisotropy field was determined by a best fit of our experimental data to the calculation result $H_A = 8.0 \pm 0.2$ kOe, thereby refining the data of Ref. 10: $H_A = 8.0 \pm 0.8$ kOe. For a more accurate comparison with experiment, the AFMR spectrum was calculated with allowance for the demagnetizing fields, since the magnetization of the EuTe crystal in fields comparable with $2H_E$ is not small ($4\pi M_0 = 116$ kOe at saturation). We note that according to our estimates the resonance-field error due to the deviation of the crystal shape from an ellipsoid does not exceed 2%. The dashed lines of Fig. 5 show the possible error corridor due to $\approx 1^\circ$ inaccuracy in the orientation of the C_4 axis of the EuTe crystal relative to the magnetic field H . It can be seen that the experimental points agree well with the calculated

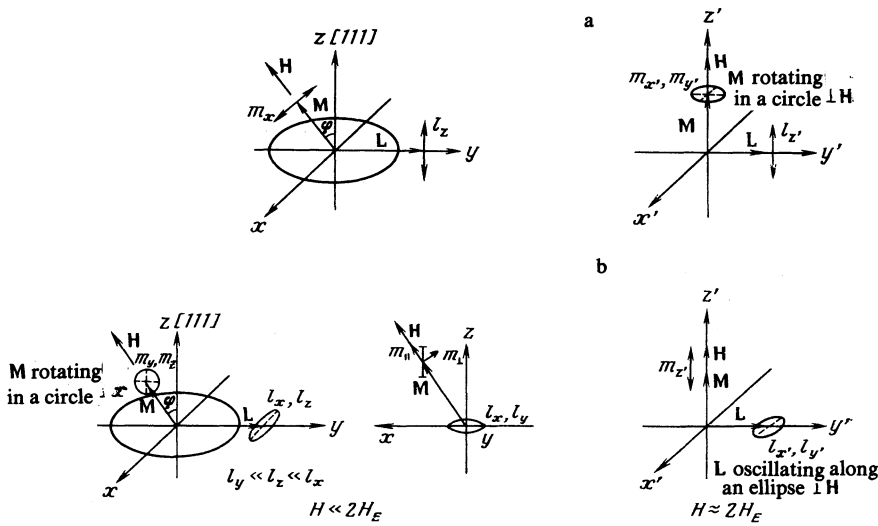


FIG. 8. Oscillation modes of the vectors \mathbf{M} and \mathbf{L} in the HF (a) and LF (b) branches of the AFMR in two limiting cases: $H \ll 2H_E$ (in the coordinates x, y, z) and $H \approx 2H_E$ (in the coordinates x', y', z').

AFMR spectrum. The gap in the spectrum of the LF branch of the AFMR, due to the weak anisotropy in the easy plane, hardly affects the resonance field at the measured frequencies 35–45 GHz. The intraplane anisotropy was therefore not determined in this experiment. The three points taken from Ref. 10 (the black dots in Fig. 5) likewise fit our calculated AFMR spectrum.

As already noted in §3, no strong-field resonance was revealed by the microwave absorption. The reason is that in both experimental geometries the exciting microwave field at the crystal was perpendicular to the static magnetic field \mathbf{H} ($\mathbf{h} \perp \mathbf{H}$, see Fig. 4), and in this case the LF branch of the AFMR was weakly excited in fields close to $2H_E$ ($\mathbf{m} \parallel \mathbf{M} \parallel \mathbf{H}$). Calculation shows that in the experimental geometry employed the weak-field-resonance energy absorbed at $\omega/2\pi = 35$ GHz is approximately 10 times higher than in strong-field AFMR.

Analysis of the experimental data (intensity and polarization) on inelastic scattering of light by AFMR excitation allows us to conclude that the dominant contribution to the elastic scattering of light in EuTe is not made by the heretofore considered magneto-optic effect (isotropic magnetic refraction). The gist of this effect is that the refractive index depends on the crystal magnetization. This question will be dealt with in detail in a separate article.

In conclusion, the authors thank L. A. Klinkova for supplying the EuTe crystals, as well as A. N. Bazhanov for measuring the EuTe magnetization.

APPENDIX

Generalized-dynamic-susceptibility tensor

We introduce the notation

$$\begin{aligned}
 B_1 &= 2H_E + H_a \sin^2 \theta + 4\pi N_x M_0, \\
 B_2 &= (2H_E + 4\pi N_y M_0) \cos^2 \theta + H_a \sin^2 \theta \cos^2 \varphi + H_a \sin^2 \theta, \\
 C_2 &= (2H_E + 4\pi N_z M_0) \sin^2 \theta - H_a \cos 2\theta, \\
 C_2 &= (2H_E + 4\pi N_z M_0) \sin^2 \theta - H_a \cos 2\theta, \\
 D &= \frac{1}{2} H_a \sin 2\varphi \sin \theta, \quad \Delta_1 = B_1 B_2 - (\omega/\gamma)^2, \\
 \Delta_2 &= C_1 C_2 - (\omega/\gamma)^2, \quad \Delta = (\omega_1^2 - \omega^2)(\omega_2^2 - \omega^2),
 \end{aligned} \tag{A1}$$

where M_0 is the magnetization at saturation,

$$\cos \theta = H^{(\text{int})} / 2H_E = H^{(\text{ext})} / (2H_E + 4\pi M_0 N_z);$$

2θ is the angle between the magnetic moments of the sublattice; H_E , H_A , and H_a are respectively the effective fields of exchange, easy-plane-anisotropy, and anisotropy in the easy plane; γ is the gyromagnetic ratio; φ is the angle between the magnetic field \mathbf{H} and the $[111]$ axis; N_x , N_y , and N_z are the demagnetizing coefficients in the $x' y' z'$ frame; ω_1 and ω_2 are the two AFMR branches defined by the equation

$$\Delta_1 \Delta_2 = B_1 C_2 O^2 \quad \text{or} \quad (\omega/\gamma)^4 - (\omega/\gamma)^2 (B_1 B_2 + C_1 C_2) + B_1 C_2 (B_2 C_1 - D^2) = 0. \tag{A2}$$

The generalized-susceptibility tensor in the $x' y' z'$ frame, which is connected with the field (see Fig. 7), is given by

$$\chi_{ij} = \frac{\gamma^2 M_0}{\Delta} \times \begin{pmatrix} B_2 \Delta_2 - D^2 C_2 & i \left(\frac{\omega}{\gamma} \right) \Delta_2 \cos \theta & - \left(\frac{\omega}{\gamma} \right)^2 D \sin \theta & -i \left(\frac{\omega}{\gamma} \right) D C_2 & \left(\frac{\omega}{\gamma} \right)^2 D \cos \theta & -i \left(\frac{\omega}{\gamma} \right) \Delta_2 \sin \theta \\ -i \left(\frac{\omega}{\gamma} \right) \Delta_2 \cos \theta & B_1 \Delta_2 \cos^2 \theta & \frac{i}{2} \left(\frac{\omega}{\gamma} \right) B_1 D \sin 2\theta & -B_1 C_2 D \cos \theta & -i \left(\frac{\omega}{\gamma} \right) B_1 D \cos^2 \theta & -\frac{1}{2} B_1 \Delta_2 \sin 2\theta \\ - \left(\frac{\omega}{\gamma} \right)^2 D \sin \theta & -\frac{i}{2} \left(\frac{\omega}{\gamma} \right) B_1 D \sin 2\theta & (C_1 \Delta_1 - B_1 D^2) \sin^2 \theta & i \left(\frac{\omega}{\gamma} \right) \Delta_1 \sin \theta & -\frac{1}{2} (C_1 \Delta_1 - B_1 D^2) \sin 2\theta & i \left(\frac{\omega}{\gamma} \right) B_1 D \sin^2 \theta \\ i \left(\frac{\omega}{\gamma} \right) D C_2 & -B_1 D C_2 \cos \theta & -i \left(\frac{\omega}{\gamma} \right) \Delta_1 \sin \theta & C_2 \Delta_1 & i \left(\frac{\omega}{\gamma} \right) \Delta_1 \cos \theta & B_1 D C_2 \sin \theta \\ \left(\frac{\omega}{\gamma} \right)^2 D \cos \theta & i \left(\frac{\omega}{\gamma} \right) B_1 D \cos^2 \theta & -\frac{1}{2} (C_1 \Delta_1 - B_1 D^2) \sin 2\theta & -i \left(\frac{\omega}{\gamma} \right) \Delta_1 \cos \theta & (C_1 \Delta_1 - B_1 D^2) \cos^2 \theta & -\frac{i}{2} \left(\frac{\omega}{\gamma} \right) B_1 D \sin 2\theta \\ i \left(\frac{\omega}{\gamma} \right) \Delta_2 \sin \theta & -\frac{1}{2} B_1 \Delta_2 \sin 2\theta & -i \left(\frac{\omega}{\gamma} \right) B_1 D \sin^2 \theta & B_1 D C_2 \sin \theta & \frac{i}{2} \left(\frac{\omega}{\gamma} \right) B_1 D \sin 2\theta & B_1 \Delta_2 \sin^2 \theta \end{pmatrix}$$

¹⁾By "low-frequency branch" of AFMR we mean the set of resonant frequencies lower than the intersection frequency ω_c (see Fig. 7). In particular, at $\varphi = 90^\circ$ this branch is found to consist of two $\omega(H)$ curves corresponding to oscillations of different symmetry.

- ¹J. Ubbink, N. J. Poulis, H. J. Gerritsen, and C. J. Gorter, *Physica (Utrecht)* **18**, 361 (1952).
²V. N. Vasyukov, A. V. Zhuravlev, S. N. Lukin, and V. T. Telepa, *Fiz. Nizk. Temp.* **9**, 429 (1983) [*Sov. J. Low Temp. Phys.* **9**, 219 (1983)].
³S. Methfessel and D. C. Mattis, *Magnetic Semiconductors*, in *Handb. d. Physik*, Vol. 18, pp. 389–562, Springer, 1968.
⁴E. L. Nagaev, *Usp. Fiz. Nauk* **117**, 437 (1975) [*Sov. Phys. Usp.* **18**, 863 (1975)].
⁵A. S. Borovik-Romanov and N. M. Kreines, *Phys. Rep.* **81**, 5 (1982).
⁶G. Bush, P. Junod, R. G. Morris, J. Muheim, and W. Stutius, *Phys. Lett.* **11**, 9 (1984).
⁷G. Will, S. J. Pickort, H. A. Alperin, and R. J. Nathans, *Phys. Chem. Solids* **24**, 1679 (1963).
⁸J. I. Kaplan, *J. Chem. Phys.* **22**, 1700 (1957).
⁹F. Keffer and W. O'Sullivan, *Phys. Rev.* **108**, 637 (1957).
¹⁰J. W. Battles and G. E. Everett, *ibid.* **B1**, 3021 (1972).
¹¹N. F. Oliveira, S. Foner, Y. Shapira, and T. B. Reed, *ibid.* **B5**, 2534 (1972).

- ¹²P. G. de Gennes, *ibid.* **118**, 141 (1960).
¹³J. Schoenes and P. Wachter, *Physica (Utrecht)* **86-88**, 125 (1977).
¹⁴N. M. Kreines, Doctoral Dissertation, Inst. Phys. Problems, 1980.
¹⁵V. S. Mandel, V. D. Voronkov, and D. E. Gromzin, *Zh. Eksp. Teor. Fiz.* **63**, 993 (1972) [*Sov. Phys. JETP* **36**, 521 (1973)].
¹⁶E. M. Lifshitz and L. P. Pitaevskii, *Statistical Physics, Part 2*, Pergamon, 1980.
¹⁷A. I. Akhiezer, V. G. Bar'yakhtar, and S. V. Peletminskii, *Spin Waves*, Wiley, 1968.
¹⁸L. D. Landau and E. M. Lifshitz, *Statistical Physics, Part 1*, Pergamon, 1980.
¹⁹A. S. Borovik-Romanov and L. A. Prozorova, *Pis'ma Zh. Eksp. Teor. Fiz.* **4**, 57 (1966) [*JETP Lett.* **4**, 39 (1966)].
²⁰E. A. Turov, *Physical Properties of Magnetically Ordered Crystals*, Academic, 1965.
²¹V. I. Ozhogin, Doctoral Dissertation, Atomic Energy Inst., Moscow, 1974.

Translated by J. G. Adashko